Scientific Research Publishing

Journal of Applied Mathematics and Physics, 2018, 6, 1614-1624
http://www.scirp.org/journal/jamp
ISSN Online: 2327-4379
ISSN Print: 2327-4352

Numerical Simulation of Interaction between Fluid and Vapor Structures in Multiphase Flow around Hydrofoil

Milan Sedlar[1], Jiri Soukal[1], Martin Komarek[1], Alexander V. Volkov[2], Artem V. Ryzhenkov[2]

[1]Centre of Hydraulic Research, Lutin, Czech Republic
[2]Moscow Power Engineering Institute, Moscow, Russia
Email: m.sedlar@sigma.cz, j.soukal@sigma.cz, m.komarek@sigma.cz, volkovav@mpei.ru, info@src-w.ru

How to cite this paper: Sedlar, M., Soukal, J., Komarek, M., Volkov, A.V. and Ryzhenkov, A.V. (2018) Numerical Simulation of Interaction between Fluid and Vapor Structures in Multiphase Flow around Hydrofoil. *Journal of Applied Mathematics and Physics*, **6**, 1614-1624.
https://doi.org/10.4236/jamp.2018.68137

Received: June 19, 2018
Accepted: August 6, 2018
Published: August 9, 2018

Abstract

This work deals with the numerical simulation of interaction of fluid and vapor structures on NACA 2412 hydrofoil during the partial cavitation oscillation. This interaction is supposed to be the most important reason for the cavity shedding when, in a certain range of the cavitation numbers, some "resonance" effect can be reached. The incidence angle is 8˚ and the Reynolds number is 1.56×10^6. The hydrofoil with the span/chord ratio of 1.25 corresponds to the experiments carried out in the cavitation tunnel. The Detached Eddy Simulation (DES) is used on full 3D geometry of the straight NACA 2412 hydrofoil to capture the strong influence of side-wall effects. Real properties of water including estimated content of undissolved air are considered to affect the compressibility of the mixture and its speed of sound. The link between strong pressure pulses during the cavity cycles and the interaction of fluid and vapor structures is discussed in detail.

Keywords

Cavitation, Fluid Structures, NACA 2412, Partial Cavitation Oscillation, DES, 3D Effects, Undissolved Air

1. Introduction

The flow inside hydraulic machines should be modeled very often as a multiphase one, though the primary fluid can be considered as the incompressible constant property liquid. One of the most common reasons is the presence of cavitation nuclei which give rise to the cavitation structures in low static pressure regions. Cavitation can result in the degradation of machine performance,

the material erosion and highly unsteady phenomena which generate unwanted noise and oscillations dangerous for the machine operation. This work concentrates on the dynamic behavior of cavitation structures occurring on the blades of hydrodynamic machines, especially pumps and inducers. Usually, at design conditions and sufficiently high cavitation numbers, the vapor structures are limited to sparsely-distributed transient cavitation bubbles travelling with the flow. Such regime is mostly steady or near-steady. At off-design conditions (and/or lower cavitation numbers) however, other cavitation mechanisms can be observed, such as a sheet cavity break-up and formation of large vapor structures. The starting conditions and typical frequencies of some cavitation instabilities in the inducers are described in studies of Brennen [1] and Tsujimoto [2]. The cavitation instabilities have been investigated experimentally and numerically also in mixed-flow pumps [3] [4] with results similar to the ones obtained with inducers. The problems of the surge instability of a cavitating propeller were studied experimentally in [5] and analyzed numerically in [6]. The studies mentioned above indicate that some (though not all) mechanisms leading to the cavitation instabilities on blades of hydraulic machines are similar to the ones causing the partial cavity instability observed on single, two-dimensional hydrofoils. Nevertheless, it has been observed that the flow and cavitation phenomena on the two-dimensional hydrofoils in cavitation tunnels have fully three-dimensional character due to the side-wall effects.

Even for tunnel flows, the detailed experimental research (both the visualizations and velocity measurements) is very complicated due to the presence of large amount of cavitation bubbles. That is why CFD becomes an important tool, attempting to capture the interaction of cavitation structures with the re-entrant jet, which is supposed to be the most important reason for the cavity shedding when, in a certain range of the cavitation numbers, some "resonance" effect can be reached [7] [8] [9]. Many of these simulations are based on two-dimensional models or 3D geometry simplified with the symmetry or periodic boundary conditions used in the span-wise direction, especially in the case of the Large Eddy Simulations (LES) which are extremely CPU-time and memory demanding. However, in many cases application of the periodicity or symmetry conditions for the Scale-Resolving Simulations (SRS) should be avoided, as the application of these conditions imposes constraints onto the resolved scales. In addition, the simplified simulations are not able to capture the strong side-wall effects which can be observed experimentally as well as numerically and which result in the dependence of the flow and cavitation phenomena on the tunnel span/chord ratio. That is why the full tunnel geometry including the side walls can be found in recent works [10], even for the Large Eddy Simulations.

2. Case Description

The presented simulations are based on the measurements and visualizations

which have been performed in the cavitation tunnel at the Centre of Hydraulic Research, Czech Republic [11]. The facility is a horizontal plane water tunnel for isolated hydrofoils (**Figure 1**). The rectangular test section has inner dimensions 150 × 150 × 500 mm. All the walls of the test section are made of organic glass to facilitate visualization from all sides. The tested NACA 2412 hydrofoil had a chord length C = 120 mm, which gives the maximum span/chord ratio S/C = 1.25.). The incidence angle was 8˚, which enabled to reach the regimes of stable partial cavity oscillation. As the main attention was focused on the dependence of cavitation dynamics on the cavitation number, the investigation has been performed for a constant Reynolds number of 1.56×10^6 and a range of cavitation number from 1.29 to 1.9. The Reynolds and cavitation numbers are defined as

$$Re = \frac{u_{\text{ref}} \times C}{\nu} \tag{1}$$

$$\sigma = \frac{p_{\text{ref}} - p_{\text{v}}}{0.5\rho u_{\text{ref}}^2} \tag{2}$$

where u_{ref} and p_{ref} are the reference velocity and static pressure at the inlet of the test section, C is the hydrofoil chord length, p_{v} is the equilibrium vapor pressure, ν is the liquid kinematic viscosity and ρ is the density of the liquid.

The presented numerical study concentrates on the span/chord ratio S/C = 1.25 though the span/chord ratios 0.417 and 0.625 have been also considered. The reason will be clarified in detail later on in the next paragraphs, but in short, the span/chord ratio S/C = 1.25 gives the possibility to capture the strong

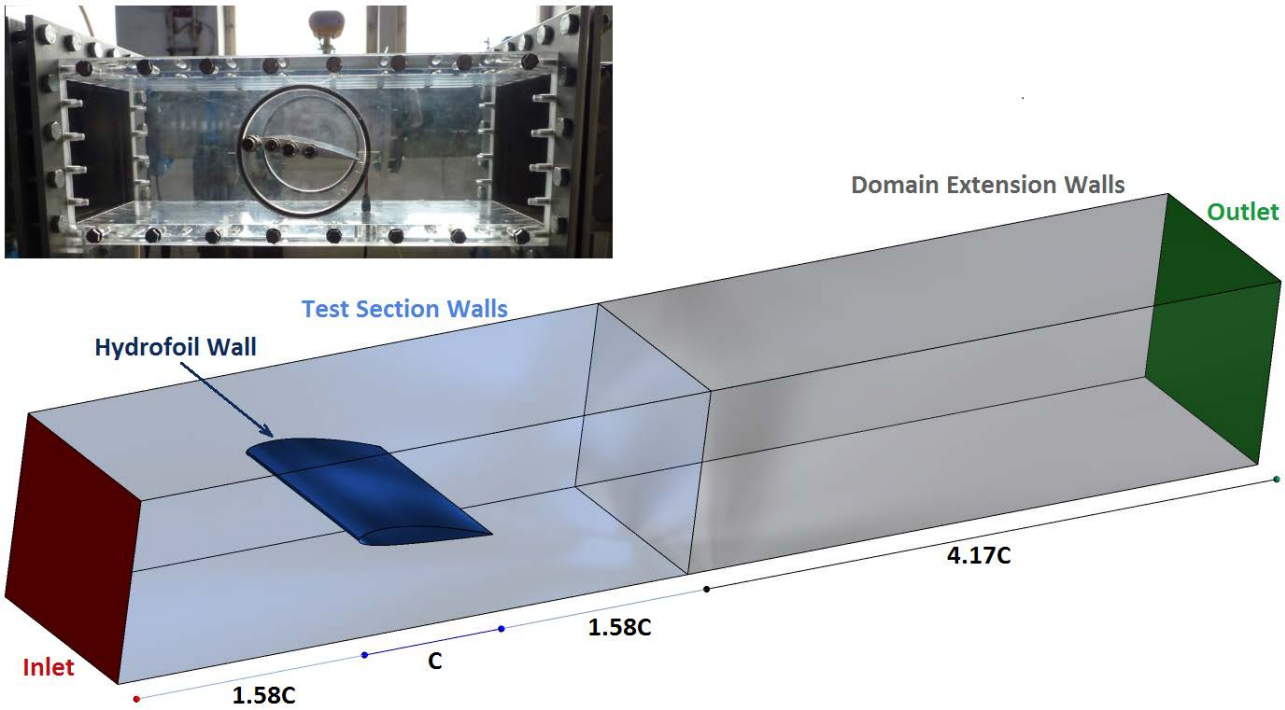

Figure 1. Geometry of the cavitation tunnel test section (top) and computational domain with straight rear extention (bottom).

side-wall effects and at the same time the core cavitation structures are well developed and not strongly stabilized by these side-wall effects. That is why the full geometry of the tunnel test section including both side walls is included into the computational domain. This paper does not focus on the details of the experiment and detailed description of the numerical procedure; these details can be found in [11]. In this reference three SRS turbulence models were tested (SAS, LES-WALE and DES). As the DES turbulence model gave the best compromise between the detailed description of the flow and cavitation structures and capturing the side wall effects, this study uses only results from DES model. As a numerical tool, the ANSYS CFX package has been used including the default (Zwart [12]) cavitation model in the ANSYS CFX package to describe the interphase mass transfer in the framework of the homogenous multiphase model.

The simulations in [11] show, that the physical models based on the incompressible constant property liquid (water) over-predict the sharp high-pressure peaks during the collapses of the bubble clouds as well as the speed of pressure pulse propagation. In this study, the real properties of water including estimated content of undissolved air are therefore considered to affect the compressibility of the mixture and its speed of sound. The volume fraction of the undissolved air at the water is set to 0.1%. The hydrofoil wall is considered to be adiabatic, the test section walls keep the constant temperature.

In both the experiments and the CFD analysis sheet cavities formed on the hydrofoil are small and relatively stable when σ is sufficiently high. Consequently, it is practically impossible to detect any regular shedding cycles and amplitudes of pressure pulses on the hydrofoil are very low. With decreasing cavitation number, it is possible to observe partial cavitation oscillation with a dominant frequency about 15 Hz. In this regime we can see dramatically increasing amplitudes of pressure pulses. **Figure 2** shows normalized amplitudes of pressure pulses measured at midspan of the hydrofoil at 40% of the chord length as a function of the normalized cavitation number. For quite a narrow range of the

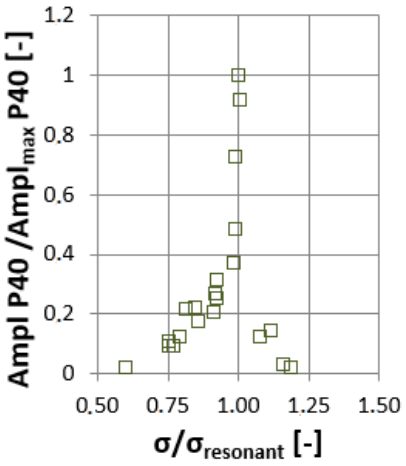

Figure 2. Amplitude (normalized) of pressure pulses at midspan of hydrofoil, 40% of cord length. Experiment.

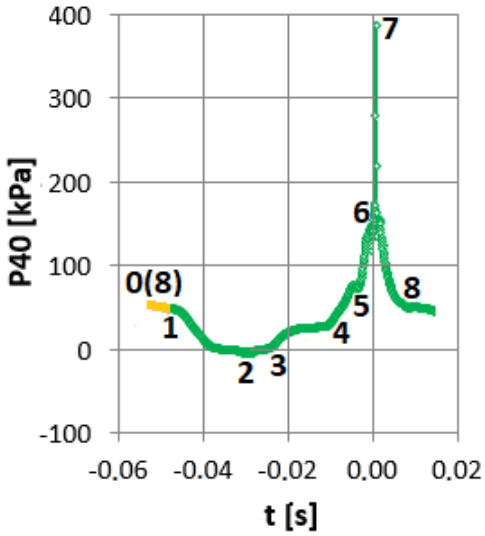

Figure 3. Pressure pulse during one shedding cycle and description of stages for **Figure 4**. CFD analysis

cavitation number the "resonance" region can be found, in which the pressure pulses reach values up to 400 kPa. CFD results indicate increased pressure pulses in the range of σ from about 1.16 to 1.71 while experiments give quite narrow "resonance" region in the range of σ from about 1.37 to 1.87, with a distinct maximum at $\sigma_{resonant} = 1.71$. This value has been taken therefore as the reference value for further numerical simulations. In the experiments, the resonant regime is quite narrow (in terms of σ), and during repeated test $\sigma_{resonant}$ was changing in the scope ± 10%, in spite of very careful setting of experiment conditions. **Figure 3** shows pressure pulse during one typical shedding cycle calculated for the cavitation number $\sigma_{resonant} = 1.71$.

Further drop of σ causes decrease of the amplitudes and in the end, for sufficiently low values of σ, a surprisingly stable super-cavitation regime starts in which it is impossible to detect any dominant frequencies. In this regime the backflow on the suction side of the hydrofoil is suppressed by intensive cavitation and practically vanishes.

3. Mechanism of the Partial Cavity Oscillation

Though we consider the beginning of the cavity shedding cycle connected with the first appearance of the re-entrant flow (Stage 1 in **Figure 3**) we just start the discussion with the Stages 0 and 8, which represent an equilibrium state in which a stable sheet cavity is developed behind the leading edge. In this paragraph we will refer to **Figure 4** (3D view of cavitation regions, reverse flow regions and vortices) and **Figure 5** (streamlines on suction surface of hydrofoil and the pressure gradient on the suction surface of hydrofoil).

Vortical structures in **Figure 4** are based on the Q criterion, which is defined in terms of the absolute values of the vorticity and the strain rate in the following way [13].

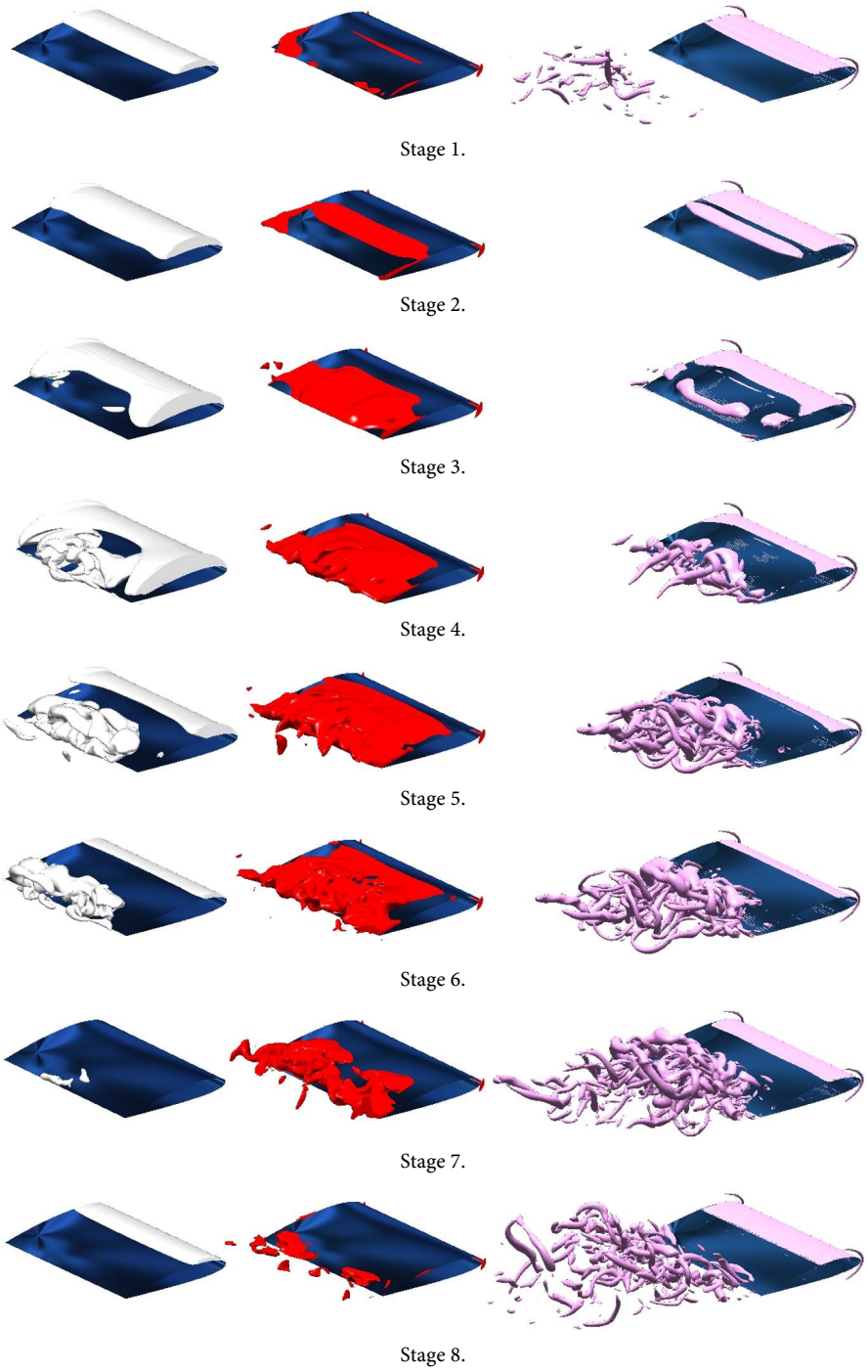

Figure 4. 3D view of cavitation regions (in white), reverse flow regions (in red) and vortices (in magenta). Stages 1 - 8. Flow direction from top right.

$$Q_{Dim} = 0.5(\Omega^2 - S^2) \tag{3}$$

$$S = \sqrt{2S_{ij}S_{ij}};\ \Omega = \sqrt{2S\omega_{ij}\omega_{ij}};\ S_{ij} = \frac{1}{2}\left(\frac{\partial U_i}{\partial x_j} + \frac{\partial U_j}{\partial x_i}\right);\ \omega_{ij} = \frac{1}{2}\left(\frac{\partial U_i}{\partial x_j} - \frac{\partial U_j}{\partial x_i}\right) \tag{4}$$

Stage 0 (physically equivalent to Stage 8) is very similar to the stable regimes which occur at higher cavitation numbers. The sheet cavity has a convex shape

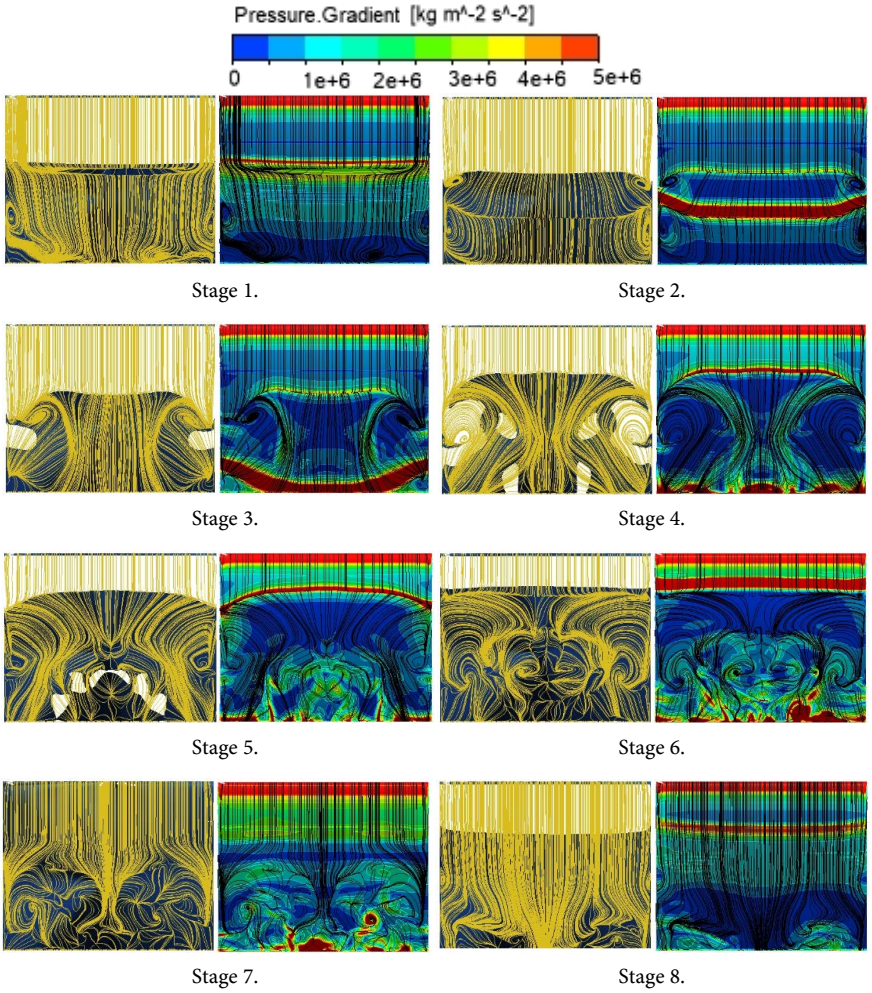

Figure 5. Left pictures: surface streamlines on suction surface of hydrofoil (in yellow) and interface between hydrofoil and cavitation regions (in white). Right pictures: pressure gradient on suction surface of hydrofoil and surface streamlines (in black). Stages 1 - 8. Flow direction from top.

and there is only one line close to the cavity closure with increased pressure gradient. Only small reverse flow regions can be found close to the trailing edge resulting from the previous cycle. Stage 1 shows the real beginning of the process, which results in the periodic cavity breakup. The sheet cavity is practically two-dimensional in the spanwise direction. At about 40% of the chord length (just behind the interface of the cavitation region and hydrofoil surface – later referred as CR-HS) we can detect a beginning of the re-entrant jet and two lines with increased pressure gradient. In Stage 2 the sheet cavity starts to become concave, at least close to the side walls, and the main reverse flow region increases. The main reverse flow region reaches the trailing edge in Stage 3 and the re-entrant flow becomes fully developed. The sheet cavity becomes significantly concave and loses its stability, which results in formation of kernels of cloud cavitation in the rear part of the hydrofoil. During Stage 4 the cavity close to the side walls reaches its maximum width. The cavitation clouds increase and in

Stage 5 reach their maximum while the sheet cavity closure starts to move towards the leading edge. Also, the reverse flow region reaches its maximum. In Stage 6, the most important effect is forming of nonzero distance between the separation line and the CR-HS interface closure. In Stage 7 the high-pressure peak is accompanied with the suppression of the sheet cavity and the decay of the re-entrant jet.

The partial cavity oscillation around the straight (two-dimensional) hydrofoil has its specific topology. Unlike some fully three-dimensional hydrofoils which largely stabilize the sheet cavity in a convex topology before its breakup [14], the two-dimensional hydrofoils with larger span/chord ratios (in our case S/C = 1.25) lack a fixed center of the sheet cavity closure. The central part of the cavity closure (as well as of the CR-HS interface closure) has a shape similar to a line parallel to the leading edge. Also, the central re-entrant flow (that is mainly streamwise) is not characterized by one stable saddle point (**Figure 6**), but by a separation line (identical with the CR-HS interface closure), which close to the side walls passes into separation lines of two side-entrants (that have a significant spanwise component). Both side-entrant jets are driven by a pair of primary vortices close to the side walls, each forming one saddle point on the separation line. All this topology makes the flow quite sensitive to asymmetry. It means that in this case, unlike the fully three-dimensional hydrofoils or two-dimensional hydrofoils with very low span/chord ratios, it is more important to use the computational domain with full geometry, *i.e.* without an application of the symmetry boundary condition. In the presented calculations, asymmetry of the solution is not distinct in the region of the sheet cavity; however it is visible in the highly turbulent region close to the trailing edge during formation and brakup of the cavitation clouds (**Figure 4 & Figure 5**, Stages 5 - 8).

4. Conclusions

Numerical modeling of cavitating flow around the hydrofoils or blades of hydraulic machines gives a unique possibility to look insight the structures, which are very dynamic and practically impossible to be captured in an experimental way. The presented results are based on the numerical analysis, but they have been verified in detail by experimental observations (**Figure 7**) and measurements of

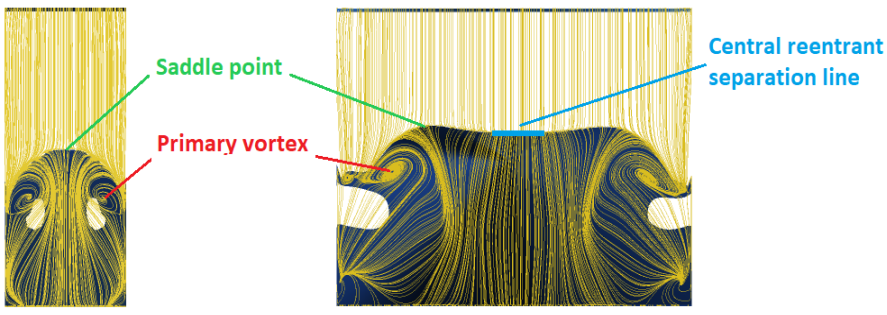

Figure 6. CR-HS interface closure and separation lines in the stage of fully developed re-entrant flow. Span/chord ratio S/C = 0.417 (left) and 1.25 (right).

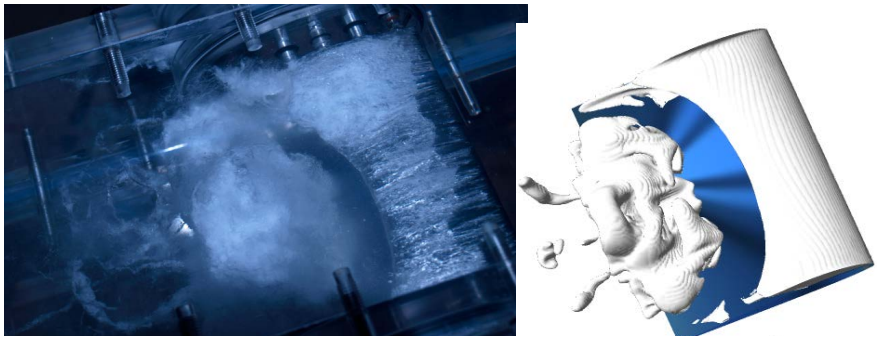

Figure 7. Comparison of cavitation structures in experimental observations and CFD simulations.

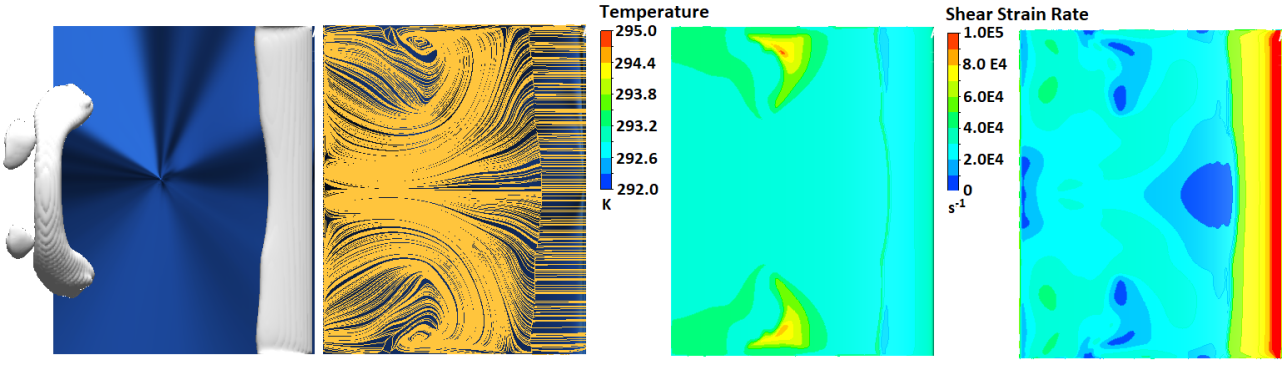

Figure 8. Calculated temperature and shear strain rate during the cavitation cloud collapse. Flow direction from right.

pressures and forces acting on the hydrofoil surfaces. The comparisons of data indicate, that the numerical simulations can give real description of all physical processes linked with these problems.

Modeling of real properties of water including estimated content of undissolved air gives the possibility to estimate better the propagation of the pressure pulses and their amplitudes. Still it is not able to consider the real bubble dynamics and the thermal processes connected with the collapse of the cavitation bubbles including their erosive potential (**Figure 8**).

The partial cavity oscillation is very important problem connected with the operation of hydraulic machines. The reason of this oscillation, which is accompanied by high pressure pulses and increased vibrations and noise, is the strong influence of the high-momentum re-entrant and side-entrant flow on the cavity interface. This mechanism depends on many factors, including the wall shear. Changing the wall surface properties, it should be possible to change (hopefully in a positive way) the dynamic behavior of the partial cavity. This task will be the main topic of research of the authors in the next future.

Acknowledgements

This work has been supported by the grant INTER-EXCELENCE No. LTARF18019 of the Ministry of Education, Youth and Sports of the Czech Republic entitled "Design of Hydraulic Micro-Sources for Energy Recuperation".

Conflicts of Interest

The authors declare no conflicts of interest regarding the publication of this paper.

References

[1] Brennen, C.E. (2013) A Review of the Dynamics of Cavitating Pumps. *Journal of Fluids Engineering*, **135**, 061301. https://doi.org/10.1115/1.4023663

[2] Tsujimoto, Y. (2007) Cavitation Instabilities in Turbopump Inducers. In: Dagostino, L. and Salvetti, M.V., Eds., *Fluid Dynamics of Cavitation and Cavitating Turbopumps*, Springer, Vienna, 169-190. https://doi.org/10.1007/978-3-211-76669-9_3

[3] Kobayashi, K. and Chiba, Y. (2010) Computational Fluid Dynamics of Cavitating Flow in Mixed Flow Pump with Closed Type Impeller. *Int. Journal of Fluid Machinery and Systems*, **3**, 113-121. https://doi.org/10.5293/IJFMS.2010.3.2.113

[4] Sedlar, M., Sputa, O. and Komarek, M. (2012) CFD Analysis of Cavitation Phenomena in Mixed-Flow Pump. *Int. Journal of Fluid Machinery and Systems*, **5**, 18-29. https://doi.org/10.5293/IJFMS.2012.5.1.018

[5] Duttweiler, M.E. and Brennen, C.E. (2002) Surge Stability on Cavitating Propeller. *Journal of Fluids Mechanics*, **458**, 133-152. https://doi.org/10.1017/S0022112002007784

[6] Watanabe, S. and Brennen, C.E. (2003) Dynamics of a Cavitating Propeller in a Water Tunnel. *Journal of Fluids Engineering*, **125**, 283-292. https://doi.org/10.1115/1.1524588

[7] Roohi, E., Zahiri, A.P. and Pasandideh-Fard, M. (2013) Numerical Simulation of Cavitation around a Two-Dimensional Hydrofoil Using VOF Method and LES Turbulence Model. *Applied Mathematical Modelling*, **37**, 6469-6488. https://doi.org/10.1016/j.apm.2012.09.002

[8] Ji, B., Luo, X., Arnd, R.E.A and Wu, Y. (2014) Numerical Simulation of Three Dimensional Cavitation Shedding Dynamics with Special Emphasis on Cavitation–Vortex Interaction. *Ocean Engineering*, **87**, 64-77. https://doi.org/10.1016/j.oceaneng.2014.05.005

[9] Wu, X.C., Wang, Y.W. and Huang, C.G. (2016) Effect of Mesh Resolution on Large Eddy Simulation of Cloud Cavitating Flow around a Three-Dimensional Twisted Hydrofoil. *European Journal of Mechanics—B/Fluids*, **55**, 229-240. https://doi.org/10.1016/j.euromechflu.2015.09.011

[10] Huang, B., Zhao, Y. and Wang, G. (2014) Large Eddy Simulation of Turbulent Vortex-Cavitation Interactions in Transient Sheet/Cloud Cavitating Flows. *Computers and Fluids*, **92**, 113-124. https://doi.org/10.1016/j.compfluid.2013.12.024

[11] Sedlar, M., Ji, B., Kratky, T., Rebok, T. and Huzlik, R. (2016) Numerical and Experimental Investigation of Three-Dimensional Cavitating Flow around a Straight NACA2412 Hydrofoil. *Ocean Engineering*, **123**, 357-382. https://doi.org/10.1016/j.oceaneng.2016.07.030

[12] Zwart, P.J., Gerber, A.G. and Belamri, T. (2004) A Two-Phase Flow Model for Predicting Cavitation Dynamics. *Proceedings of International Conference on Multiphase Flow*, Jokohama, 30 May-3 June, No. 152.

[13] Menter, F.R., Schutze, J. and Kurbatskii, K.A. (2011) Scale-Resolving Simulation Techniques in Industrial CFD. *Proceedings of the* 6*th AIAA Theoretical Fluid Mechanics Conference,* AIAA, Honolulu, 27-30 June 2011, 2011-3474.

https://doi.org/10.2514/6.2011-3474

[14] Foeth, E.J., van Doorne, C.W.H., van Terwisga, T. and Wieneke, B. (2008) On the Collapse Structure of an Attached Cavity on a Three-Dimensional Hydrofoil. *Journal of Fluids Engineering*, **130**, 071303. https://doi.org/10.1115/1.2928345